To cite this article: WANG H T, XIANG G, YUAN Z S, et al. Numerical study on hydrodynamic performance of ducted propeller based on improved body force model[J/OL]. Chinese Journal of Ship Research, 2023, 18(4). http://www.ship-research.com/en/article/doi/10.19693/j.issn.1673-3185.02920.

DOI: 10.19693/j.issn.1673-3185. 02920

Numerical study on hydrodynamic performance of ducted propeller based on improved body force model

WANG Haotian[1], *XIANG Gong*[*1,2,3,4], *YUAN Zaisi*[1], *XIANG Xianbo*[1,3,4]

1 School of Naval Architecture and Ocean Engineering, Huazhong University of Science and Technology, Wuhan 430074, China

2 State Key Laboratory of Fluid Power and Mechatronic Systems, Zhejiang University, Hangzhou 310027, China

3 Key Laboratory of Ship and Ocean Hydrodynamics of Hubei Province, Huazhong University of Science and Technology, Wuhan 430074, China

4 Collaborative Innovation Center for Advanced Ship and Deep-Sea Exploration, Shanghai 200240, China

Abstract: [**Objectives**] The paper aims to solve the limitations of the Goldstein body force method in a hydrodynamic simulation of a ducted propeller. [**Methods**] An analysis of the reason for the distortion of the duct hydrodynamic simulation is carried out based on the wing theory, and a correction method based on the mass flow and body force distribution model is proposed. The RANS method is then used to study the simulation accuracy of two kinds of improved body force methods. [**Results**] The results show that the average relative error of the total thrust coefficient of the two improved body force methods under open water conditions is about 5%. The average relative error of the resultant forward force of the two improved volume force methods behind the underwater vehicle is 1.8% and 11.6% respectively. [**Conclusions**] The simulation accuracy of a ducted propeller based on the improved body force method in open water and behind an underwater vehicle is greatly improved compared with the traditional method. The proposed method can accurately simulate the hydrodynamic performance of a ducted propeller, laying the foundation for the efficient dynamic maneuverability simulation of underwater vehicles.

Keywords: improved body force method; ducted propeller; mass flow correction; distribution correction; computational fluid dynamics (CFD)

CLC number: U661.33

0 Introduction

Both remotely operated vehicles (ROVs) and autonomous underwater vehicles (AUVs) need to be highly maneuverable to achieve pose transformation and complete tasks according to pre-set programs or real-time instructions. Computational fluid dynamics (CFD) has become an important method of investigating ship maneuverability amid the rapid development of computer technology. It can be applied to solve complex flows that cannot be obtained by theoretical analysis and requires much less human and financial resources than physical tests. However, CFD is often time-consuming in simulating multi-time-scale physical fields (such as helicopter flight and ship propeller

Received: 2022 – 05 – 13 **Accepted**: 2022 – 07 – 16

Supported by: Key Fund Program of National Natural Science Foundation of China (52131101); National Key Laboratory Open Fund on Hydrodynamic Force and Electromechanical Systems (GZKF-202001)

Authors: WANG Haotian, male, born in 1995, Ph.D. candidate. Research interest: ship and ocean engineering hydrodynamics. E-mail: ouc1924foxmail.com

XIANG Gong, male, born in 1989, associate professor, doctoral supervisor. Research interest: hydrodynamics of ships and marine structures and high-performance ships. E-mail: gongxiang@hust.edu.cn

XIANG Xianbo, male, born in 1978, professor, doctoral supervisor. Research interest: marine intelligent equipment and systems and ocean robots. E-mail: xbxiang@hust.edu.cn

***Corresponding author**: XIANG Gong

propulsion). For this reason, the body force method (BFM) is usually used to simulate the high-speed rotation of blades.

The BFM is also known as the momentum source method (MSM) or the actuator disk theory (ADT) in different disciplinary fields [1]. In the BFM, the force exerted on a fluid by the propeller is equated with a force source term in a particular distribution form and then input into the Navier-Stokes (N-S) equation for solution. In this way, the BFM not only reduces the number of meshes and the difficulty in mesh generation but also narrows the span of the time scales of the physical fields, ultimately achieving higher computational efficiency. When detailed information on the flow field is not required, this method is readily applicable to submarine maneuverability evaluation [2-3]. Gaggero et al. [4] explored the rapid design and optimization of the shape of the duct by leveraging the high computational efficiency of the BFM. He et al. [5] simulated the rotation of KRISO container ships (KCSs) by the improved BFM based on the blade element theory and achieved satisfactory accuracy. Wu et al. [2] used a body force distribution model to simulate the rotation of the KCSs numerically. Wu et al. [6] conducted a numerical study of the self-propulsion of ships by a descriptive BFM to examine the influences of the inflow disk radius and offset of a virtual propeller on self-propulsion.

Currently, the most commonly used descriptive BFM takes the Goldstein optimal circulation distribution as the distribution model. This optimal circulation distribution can be traced back to Goldstein's [7] successful and accurate solution to the problem concerning the optimal circulation distribution condition proposed by Betz on the basis of the potential-flow lifting-line theory. The performance of propellers depends on the radial circulation distribution. According to Wu et al. [8], the Goldstein optimal circulation distribution is not applicable to ducted propellers since its accuracy in simulating the hydrodynamic performance of ducted propellers is lower than the accuracy it provides in simulating ordinary propellers. Feng et al. [9] directly used the local velocity field at the propeller disk calculated by the CFD approach to calculate the thrust and torque of the blades at each radius by applying the blade element theory, thereby obtaining a flow field distribution that is almost the same as that of a discretized propeller model. Yu et al. [10] studied the internal flow of tunnel thrusters by an improved BFM and proposed a flow rate correction method considering the influence of rotor blockage. Eslamdoost et al. [11] studied the applicability of three body force models in axial flow pumps. The one taking into account the guide vanes, the axially uniformly distributed body force, and the circumferential body force achieved equivalent head accuracy to that obtained by the multiple reference frame (MRF) method and attained a local flow field at the nozzle more accurate than the one obtained by the MRF method. Knight et al. [12] trained a semi-empirical algorithm to determine an unsteady propeller body force. Song et al. [13] conducted an MSM-based CFD analysis of an air ducted tail rotor similar to an underwater ducted propeller according to the blade element theory. The results showed that the rotor thrust was basically consistent with the test value.

Currently, numerous studies have been conducted to improve the BFM, but they rarely focus on the applicability and improvement of the BFM for underwater ducted propellers. Studying the BFM readily applicable to ducted propellers is conducive to improving the efficiency in simulating the maneuverability of underwater vehicles on the premise of ensuring the macroscopic motion accuracy of the vehicles. To solve the problem concerning the limited applicability of the traditional BFM to ducted propellers, the authors primarily explain the distorted simulation of the hydrodynamic performance of the ducted propeller by applying the wing theory. Then, they propose mass flow rate and distribution correction methods. Finally, the simulation accuracy of the two forms of body force distribution is examined in open water and behind an underwater vehicle, and the improved BFMs are numerically verified. This study is expected to lay the foundation for the efficient and accurate dynamic maneuverability simulation of underwater vehicles equipped with ducted propellers.

1 Numerical simulation method

In this study, the Reynolds-averaged Navier-Stokes (RANS) method and the STAR-CCM+ solver are used to conduct a BFM-based study of the hydrodynamic performance of ducted propellers.

1.1 Control equation

In a three-dimensional steady and incompressible viscous flow field, the fluid satisfies both the

continuity equation and momentum conservation equation:

$$\frac{\partial u_i}{\partial x_i} = 0 \tag{1}$$

$$u_j \frac{\partial (u_i)}{\partial x_j} = -\frac{1}{\rho}\frac{\partial p}{\partial x_i} + (g_i + f_i) + \frac{\mu}{\rho}\frac{\partial^2 u_i}{\partial x_j \partial x_j} - \frac{\partial \overline{u_i' u_j'}}{\partial x_j} \tag{2}$$

where x_i and x_j (i, j = 1, 2, 3) are coordinate components; u_i and u_j (i, j = 1, 2, 3) are the time average of velocity components; ρ is the fluid density; p is the time average of pressure; g_i and f_i are the components of gravitational acceleration and the custom unit mass force in x_i direction, respectively; $-\overline{u_i' u_j'}$ is the Reynolds stress term; μ is the dynamic viscosity coefficient. The classical eddy viscosity assumption is adopted to express the averaged Reynolds stress tensor in the form suggested by Boussinsq:

$$-\rho \overline{u_j' u_i'} = \mu_t \left(\frac{\partial \overline{u}_i}{\partial x_j} + \frac{\partial \overline{u}_j}{\partial x_i} \right) - \frac{2}{3}\rho k \delta_{ij} \tag{3}$$

where μ_t is the turbulent eddy viscosity; k is the fluctuating turbulent kinetic energy per unit mass of the fluid; δ_{ij} is the Kronecker function. A two-equation model, namely, the shear-stress transport (SST) k-ω turbulence model readily applicable to the numerical calculation of submarine maneuverability, is used to close the RANS equation. This model has high computational accuracy for both attached boundary layer turbulences and moderately separated turbulences[14]. The transport equations for turbulent kinetic energy k and unit dissipation rate ω, as well as the definition and value of each parameter in them, can be found in References [15-16].

1.2 Computational model and mesh division

In this study, the Myring-shaped axisymmetric revolution body and the famous No. 19A duct in the Dutch ship model testing tank are selected as the research objects. The geometry of the Myring-shaped axisymmetric revolution body and the No. 19A duct is illustrated in Fig. 1. Table 1 provides the main parameters of both the axisymmetric revolution body and the duct (assembly).

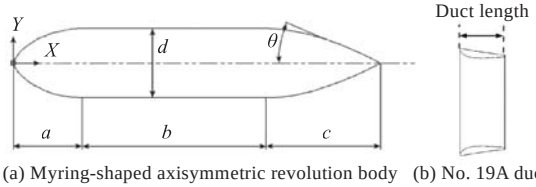

(a) Myring-shaped axisymmetric revolution body (b) No. 19A duct

Fig. 1 Geometry of revolution body and duct

Table 1 Main parameters of ducted propeller and revolution body

Parameter	Value	Parameter	Value
Propeller diameter D/mm	47.30	Revolution body diameter d/mm	94.60
Pitch ratio P/D	1	Head length a of revolution body/mm	94.60
Hub-diameter ratio	0.18	Parallel middle body length b of revolution body/mm	252.26
Number of blades	4	Tail length c of revolution body/mm	157.16
Duct length/mm	23.65	Departure angle θ at the tail of revolution body/(°)	40

The computational domain and the boundary conditions are shown in Fig. 2. The computational domain of the fluid is the region between the cuboid and the assembly, with the cuboid being 80b, 16b, and 16b in length, width, and height, respectively. The surfaces of the revolution body and the duct are all non-slip walls. The downstream boundary surface of the cuboid is a pressure outlet, while the other five surfaces are all velocity inlets. The head of the assembly is 24b away from the upstream boundary surface, 55b away from the downstream boundary surface, and 8b away from both the left and right boundary surfaces. Fig. 3 presents the mesh division and refinement of the assembly. The meshes around the revolution body and the duct are refined to accurately capture the physical quantities with large gradients. The outermost body-fitted meshes near the walls should be dimensionally equivalent to the adjacent meshes to ensure a natural transition of the meshes. Five layers of boundary-layer meshes are divided for the revolution body, with the first layer being 0.5 mm high. Four layers of boundary-layer meshes are divided for the duct, with the first layer being 0.04 mm high. The region near the propeller disk in the duct where a body force source term is applied is refined to improve the distribution accuracy of the term. Boundary-layer meshes are also divided on the walls of the duct and the revolution body to the effect that their y^+ value is around 60 on the whole.

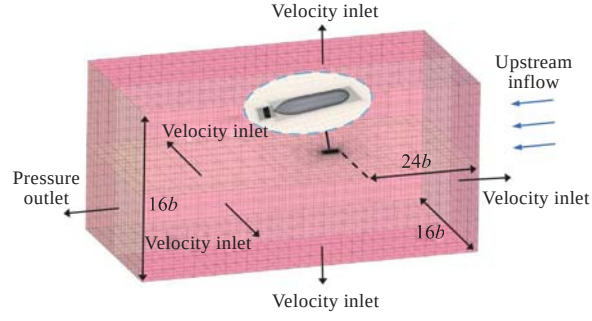

Fig. 2 Computational domain and boundary conditions

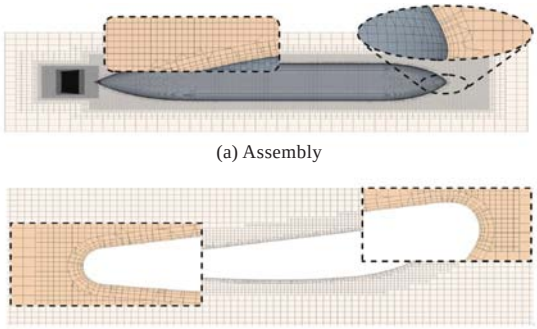

(a) Assembly

(b) Around the duct

Fig. 3 Mesh division and refinement of assembly

2 Principle and distortion analysis of traditional BFM

2.1 Principle of traditional BFM

The traditional BFM is the most commonly used descriptive BFM that takes the Goldstein optimal distribution as the distribution model, which is also known as the classic H-O model [7]. It is referred to as the "Goldstein distribution" method in this paper.

In this method, the body force is uniformly distributed along the axial direction of the cylindrical virtual disk, and its radial distribution follows the Goldstein optimal distribution:

$$f_{bx} = A_x r^* \sqrt{1-r^*} \tag{4}$$

$$f_{b\theta} = A_\theta \cdot \frac{r^* \sqrt{1-r^*}}{r^*\left(1-r_h'\right)+r_h'} \tag{5}$$

where

$$A_x = \frac{105}{8} \cdot \frac{T}{\pi \Delta (3R_H + 4R_P)(R_P - R_H)}$$

$$A_\theta = \frac{105}{8} \cdot \frac{Q}{\pi \Delta R_P (3R_H + 4R_P)(R_P - R_H)} \tag{6}$$

$$r^* = \frac{r' - r_h'}{1 - r_h'}, \quad r_h' = \frac{R_H}{R_P}, \quad r' = \frac{r}{R_P}$$

In the above equations, f_{bx} and $f_{b\theta}$ are the axial and tangential components of the body force, respectively; r is the radial coordinate; R_H is the hub radius; R_p is the tip circle radius; Δ is the virtual disk thickness; T and Q are the thrust and torque of the propeller, respectively.

2.2 Analysis of distorted simulation of open-water performance

The body force model pairing a No. 19A duct with a Goldstein-distribution propeller (hereinafter referred to as the "duct+G") is numerically simulated to investigate the accuracy and applicability of this model in numerically simulating the open-water performance of ducted propellers. The simulation scenario is illustrated in Fig. 4, where the body force source is distributed in the duct to simulate the hydrodynamic effect of a discretized propeller. In the simulation, values are taken from the open-water curve of a single Ka4-70 propeller to obtain the open-water performance curve, and the advance coefficient J is set to the design range of the ducted propeller from 0.1 to 0.7. Moreover, the rotational speed n of the BFM is kept constant at 1 500 r/min. The open-water performance curves of the duct+G obtained by simulation are shown in Fig. 5(a). In the figure, K_{TPG} and K_{TDG} are the thrust coefficients of the propeller and the duct, respectively, and K_{TP0} and K_{TD0} are the corresponding test values [17].

Fig. 4 Spatial distribution of body force source

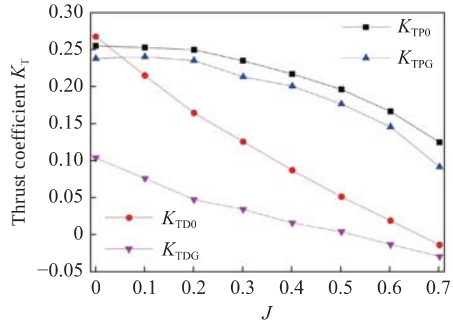

(a) Thrust coefficient

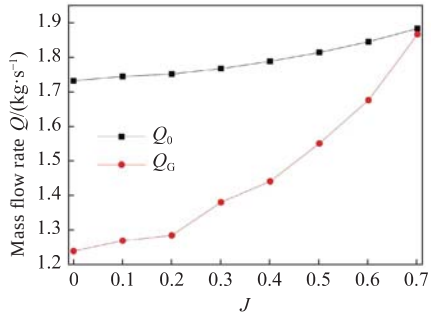

(b) Mass flow rate (n = 1 500 r/min)

Fig. 5 Open-water performance curves of No.19A duct propeller with Goldstein-distribution

As can be seen from Fig. 5(a), the thrust coefficient of the propeller follows the same trend as that

of its test value, with an average relative error of −8%. In contrast, the thrust coefficient of the duct follows a trend that is far from that of its test value, with an average relative error of over 50%. The forces acting on the duct are analyzed to determine the reasons for the low accuracy of the simulated thrust of the duct. The flow field around the duct and the analysis of the forces on the duct section are shown in Fig. 6. In the figure, F_L and F_D are the lift and drag on the airfoil, respectively, and F is the resultant force. The No. 19A duct is of an accelerating type as it can accelerate the water flow into the propeller disk, resulting in a flow field characterized by a relatively high flow velocity inside the duct and a relatively low flow velocity outside the duct. Fig. 6(b) presents the inflow velocity V_A on the duct section under the joint action of the duct and the propeller. The duct section can be considered as an airfoil with an attack angle α, which increases with the ratio between the axial flow velocities inside and outside the duct, and vice versa. When the attack angle α is large, the axial component T_D of the resultant force F points upstream. In this case, the duct thrust T_D is in the advancing direction. When the attack angle is a particular value that enables the resultant force F to be in the radial direction, the duct thrust T_D is zero. Similarly, when the attack angle is small, a negative thrust pointing downstream will be generated from the duct. Therefore, the duct thrust is related to the hydrodynamics of the duct-propeller interaction. However, the interaction between the duct and the propeller is not considered in the Goldstein-distribution BFM, resulting in a significant difference between the simulation and test values of the duct thrust coefficient.

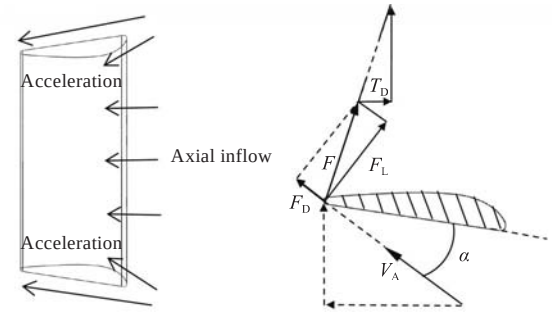

(a) Flow field around duct (b) Analysis of forces on duct section

Fig. 6 Hydromechanic analysis of duct

The magnitude of the attack angle (or the ratio between the axial flow velocities inside and outside the duct) affects the lift-to-drag ratio of the airfoil to the effect that it affects the magnitude of the duct thrust T_D. The mass flow rate of the fluid inside the duct is a macroscopic characterization of the ratio between the axial flow velocities inside and outside the duct. The flow rate Q_G inside the ducted propeller under different advance coefficients is shown in Fig. 5(b), where Q_0 is the numerical simulation result of a discretized No. 19A+Ka4-70 ducted propeller. According to the figure, Q_G is much smaller than Q_0, indicating a significant difference between them. This difference decreases as the advance coefficient J increases, following the same variation trend as that of the difference between the duct thrust coefficient and the test value. A larger advance coefficient leads to a smaller difference in the mass flow rate and ultimately to a smaller relative error in the duct thrust coefficient. This phenomenon is consistent with the above analysis of the reasons for the low accuracy of the simulated duct thrust. The difference in the mass flow rate may be related to rotor blockage.

3 Improved BFM

As mentioned in the last section, the inaccurate thrust simulation can be attributed to the failure of the Goldstein-distribution BFM to consider the interaction between the duct and the propeller. In this study, corrective measures will be proposed from two aspects, namely, the mass flow rate and body force distribution, to improve the traditional BFM.

3.1 Correction of mass flow rate

In this study, the conventional advance coefficient J is replaced with the corrected advance coefficient J^* in the calculation of the propeller advance coefficient to achieve mass flow rate correction. The corrected advance coefficient J^* is expressed as follows:

$$J^* = \frac{V_A^*}{nD} = \frac{V_{\text{InflowPlane}} - \lambda V_{\text{induced}}}{nD} \tag{7}$$

In other words, the correction coefficient λ for the flow rate is introduced before the induced velocity V_{induced}. In this case, the corrected advance velocity can be obtained by subtracting λ times the induced velocity, namely, $\lambda V_{\text{induced}}$, from the velocity $V_{\text{inflowPlane}}$ on the inflow plane. When $\lambda \equiv 0$, the coefficient is the conventional advance coefficient J without mass flow rate correction. Two simplifications are made in this study: Only the axial induced velocity is considered; the induced velocity

includes those induced by both the propeller and the duct. The mass flow rate Q is defined as follows:

$$Q = \rho S V_{\text{InflowPlane}} \tag{8}$$

where S is the area of the inflow plane (flow cross-section).

According to the definitions of both the corrected advance coefficient J^* and the mass flow rate Q in Eqs. (7) and (8), the momentum theorem suggests that the increment in the axial velocity at the propeller disk, namely, $|\Delta V_{\text{Inflow}}|$, is smaller than that at the duct outlet, namely, $|\Delta V_{\text{induced}}|$, when the rotational speed of the propeller and the distant inflow velocity (navigation speed) remains constant and the accelerating ducted propeller (body force) rotates forward. Clearly, when $\lambda > 1$, the variation in the advance velocity on an inflow plane (propeller disk) caused by the presence of λ, i.e., $|\Delta V_{\text{Inflow}}|$, is always smaller than the variation in the induced velocity caused by the presence of λ, i.e., $|\Delta\lambda V_{\text{induced}}|$. Therefore, when $\lambda > 1$, the corrected advance velocity V_A^* decreases, namely that J^* decreases. In this case, the propeller thrust coefficient increases, and the body force source term increases accordingly, leading to an increase in the velocity $V_{\text{flowPlane}}$ on the inflow plane and the mass flow rate Q (the duct thrust coefficient). As shown in Fig. 5, this is also the desired correction effect for the present study.

The correction coefficient λ for the flow rate can be solved as follows:

1) The numerical relationship $Q_0 = f(V)$ between the navigation speed V and Q_0 of the discretized ducted propeller at a particular rotational speed is obtained by numerical simulation;

2) The numerical relationship $\lambda = g(V, Q)$ among λ, V, and mass flow rate Q of the duct+ body force model is obtained by numerical simulation as well;

3) The real-time navigation speed v obtained by numerical solution is interpolated to determine Q_0, which is then substituted into $\lambda = g(v, Q_0)$ to obtain $\lambda = g(v, f(v))$ by interpolation.

The implementation process of the improved BFM after correction is shown in Fig. 7. The modified or newly added steps are highlighted in dashed boxes to underline the differences between this process and the one of the traditional BFM.

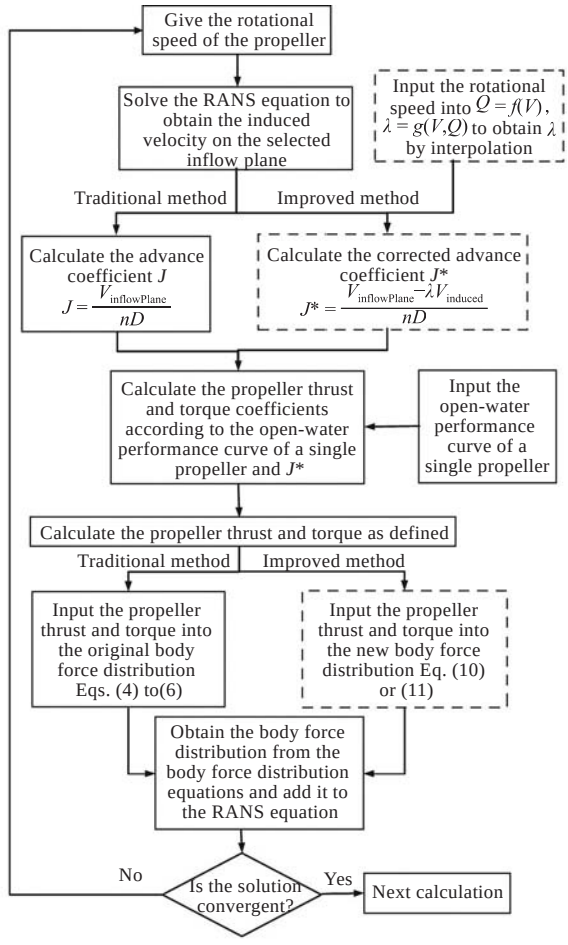

Fig. 7 Flow chart of Goldstein-distribution method and improved BFM

3.2 Correction of body force distribution

The flow velocity distribution around the duct wall has a significant influence on the hydrodynamic performance of the duct. Under a generally equivalent mass flow rate, different forms of body force distribution can still affect the magnitude of the thrust T_D from the duct by changing the flow velocity around the duct. Therefore, an appropriate body force distribution is required.

The distribution of the thrust generated by the discretized No.19A+Ka4-70 ducted propeller along the normalized radius r^* under each advance coefficient is obtained by numerical simulation. Then, the body force distribution corresponding to the propeller thrust is obtained by body weighting at each radius. Finally, the body force distribution obtained is compared with the Goldstein optimal distribution. The normalized radius r^* can be expressed as

$$r^* = \frac{r - R_H}{R_P - R_H} \tag{9}$$

The radial division form of the propeller and the body force distribution under each normalized radius of the propeller are shown in Fig. 8. In the figure, the body force f is normalized at its maximum value $f_{\max}$. When $r^* \leqslant 0.65$, the body force distribution curve of thediscretized ducted propeller is similar to the Goldstein optimal distribution;

when $r^* \geqslant 0.65$, the normalized body force of the discretized ducted propeller decreases. Moreover, it attenuates faster under a larger advance coefficient J but basically remains larger than 0.6. In contrast, the body force in the Goldstein optimal distribution is smaller than the simulation value when $r^* \geqslant 0.8$ and is 0 when $r^* = 1$ (blade tip). The characteristics of the body force distribution of the discretized ducted propeller differ substantially from those of the Goldstein optimal distribution. The results are consistent with those in Reference [8].

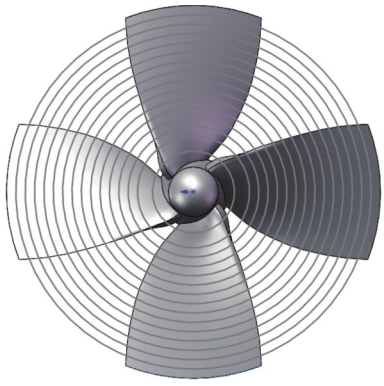

(a) Radial division of ducted propeller blades

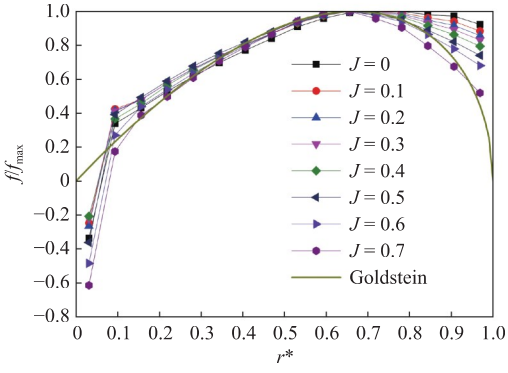

(b) Body force distribution of propeller under each normalized radius

Fig. 8 Radial division form of ducted propeller and its body force distribution under each normalized radius

The applicability of two forms of body force distribution in the simulation of the hydrodynamic performance of a ducted propeller is studied according to the characteristics of the normalized body force distribution of the propeller.

1) Simple uniform distribution.

$$\frac{f}{f_{\max}} = 1 \tag{10}$$

2) The normalized body force of the propeller follows a similar trend under each advance coefficient J. For this reason, one of them (the body force distribution in the case of $J = 0.4$ is taken in this study) is selected to replace the Goldstein optimal distribution for the correction of body force distribution. After curve fitting, the corrected body force distribution is expressed as follows:

$$\frac{f}{f_{\max}} = \sum_{i=0}^{6} a_i (r^*)^i \tag{11}$$

where a_i is a coefficient and is set to $a_0 = 0.541\ 9$, $a_1 = 16.443$, $a_2 = -50.745$, $a_3 = 129.8$, $a_4 = -168.74$, $a_5 = 91.85$, and $a_6 = -15.435$, respectively.

4 Verification of calculation methods

4.1 Verification of open-water thrust from discretized ducted propellers

The No. 19A+Ka4-70 (P/D =1) ducted propeller is numerically simulated, and the simulation results of duct thrust and propeller thrust are compared with the test values to verify the rationality of the calculation methods. The geometric model and mesh refinement region of the ducted propeller are shown in Fig. 9. The computational domain consists of one covering the duct and another cylindrical one covering the propeller. The axis of the cylinder coincides with that of the propeller, and the side and two bottoms of the cylinder are the internal interfaces between the two computational domains. The gap between the propeller and the duct, the leading and trailing edges, and the region near the blades are refined to capture rapidly changing physical quantities. Three sets of meshes are obtained by adjusting the meshes on and in the vicinity of the wall of the ducted propeller. The rotation of the propeller is simulated by applying the MRF. The simulation and test results of the thrusts are compared in Table 2. As can be seen from the table, the relative errors in the propeller thrust coefficient K_{TP} and the duct thrust coefficient K_{TD} follow a decreasing trend on the whole as the number of meshes increases. The simulated absolute K_{TD} is relatively consistent with the test value, but the relative error between them is slightly large because the duct thrust coefficient has a small absolute value and is sensitive to errors; the relative

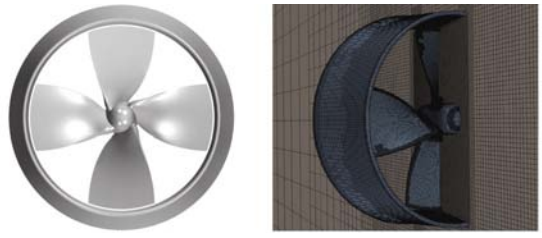

(a) Geometric model (b) Mesh refinement region

Fig. 9 Geometric model and mesh division of No.19A+Ka4-70 (P/D = 1) ducted propeller

Table 2 Verification of thrust calculation method for ducted propeller

Advance coefficient J		Simulated thrust coefficient			Test value	Relative error/%		
		Mesh 1 (1.09 million)	Mesh 2 (160 million)	Mesh 3 (194 million)		Mesh 1	Mesh 2	Mesh 3
Propeller thrust coefficient	0.1	0.247 6	0.252 6	0.253 2	0.252 4	−1.892	0.053	0.287
	0.3	0.224 5	0.229 5	0.230 1	0.234 6	−4.301	−2.196	−1.940
	0.6	0.153 7	0.161 2	0.162 1	0.166 3	−7.591	−3.089	−2.548
Duct thrust coefficient	0.1	0.189 8	0.202 9	0.202 9	0.214 8	−11.610	−5.550	−5.543
	0.3	0.100 1	0.110 6	0.111 3	0.125 7	−20.340	−12.040	−11.480
	0.6	0.009 3	0.017 4	0.017 5	0.018 8	−50.520	−7.549	−7.123

error in K_{TP} is below 5% and is within the allowable range. Considering both computational cost and accuracy, the authors adopt the relevant settings of Mesh 2 for the ducted propeller hereunder.

4.2 Verification of resistance on revolution body

To study the overall hydrodynamic performance of an interacting revolution body and ducted propeller, the authors need to verify the simulation method for the hydrodynamic performance of the revolution body. The Myring-shaped axisymmetric revolution body of the "Assembly 1" type with test data in Reference [18] is numerically simulated. Three sets of meshes are obtained by refining the meshes on and in the vicinity of the wall of the revolution body. The results shown in Table 3 are obtained by comparing the simulation results with the test values. According to Table 3, the simulated resistance on the revolution body under each navigation speed agrees well with the test values. As the number of meshes increases, the relative error gradually decreases. Mesh b has a maximum relative error of −7.727%, and the corresponding simulation results are within the allowable error range and are close to those of Mesh c. For the sake of both computational cost and accuracy, the relevant settings of Mesh b are used hereunder.

Table 3 Verification of calculation method for resistance on revolution body

Inflow velocity/kn	Simulatex resistance on revolution body/N			Test value/N	Relative error/%		
	Mesh a(0.45 million)	Mesh b(1.07 million)	Mesh c(1.43 million)		Mesh a	Mesh b	Mesh c
0.3	0.355 5	0.372 9	0.373 2	0.379 1	−6.237	−1.648	−1.569
0.5	0.877 8	0.909 2	0.909 5	0.940 0	−6.617	−3.276	−3.244
0.7	1.605 0	1.644 0	1.646 0	1.706 0	−5.903	−3.593	−3.476
0.9	2.528 0	2.574 0	2.577 0	2.790 0	−9.362	−7.727	−7.616

5 Calculation results and analysis

5.1 Open-water hydrodynamic performance of ducted propeller based on improved BFM

The hydrodynamic performance of the No.19A+ Ka4-70 ducted propeller in open water is numerically simulated using improved BFMs whose flow rate and distribution have been corrected. The propeller thrust coefficient K_{TP}, the duct thrust coefficient K_{TD}, and the mass flow rate Q are shown in Fig. 10. The subscripts 0, G, 1, and 2 represent the test values [17], the Goldstein optimal distribution, the distribution defined by Eq. (10) (uniform distribution, referred to as "Distribution 1"), and the distribution defined by Eq. (11) (referred to as "Distribution 2"). For the convenience of description, the improved BFM in a uniform distribution after flow rate correction is referred to as the improved BFM 1, and the one in Distribution 2 after flow rate correction is referred to as the improved BFM 2.

An overview of Fig. 10 reveals that the parameters of the ducted propeller obtained by the improved BFMs 1 and 2 all agree well with the test values. Specifically, the average relative errors in propeller thrust coefficient K_{TP} obtained by the two methods are 7.8% and 10%, respectively, and are thus slightly better than those in the values obtained by the Goldstein-distribution method (the average relative error in the K_{TP} obtained by this method is 10%); the relative errors in duct thrust coefficient

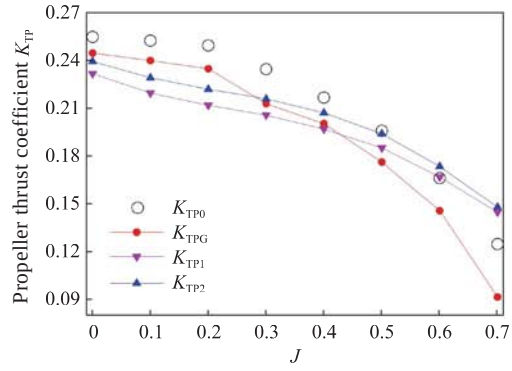

(a) Propeller thrust coefficient

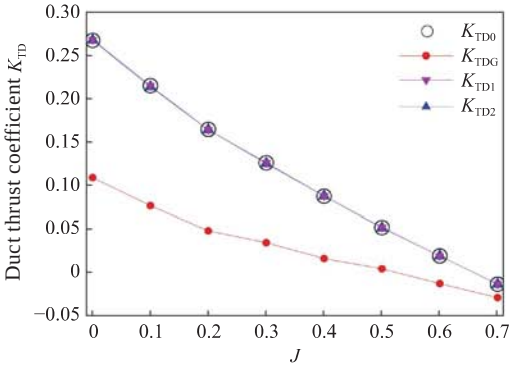

(b) Duct thrust coefficient

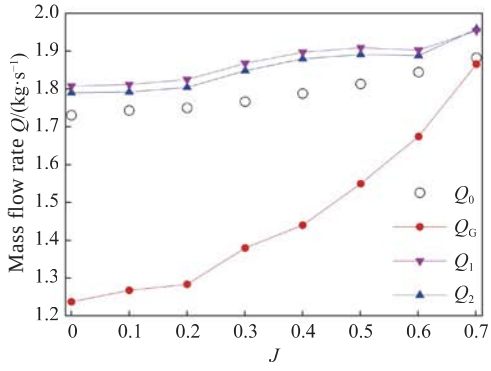

(c) Mass flow rate

Fig. 10 Comparison of open-water performance curves of ducted propeller based on improved BFMs

K_{TD} are about 0.1%. The above results indicate that both the two improved models can effectively solve the problem concerning the inaccurate hydrodynamic simulation of the duct. The mass flow rate Q obtained by the improved BFMs 1 and 2 follows the same trend as that of the test value, and the average relative errors are 4.5% and 3.7%, respectively, which are within the acceptable range in engineering. In contrast, the absolute average relative errors in K_{TD} and Q obtained by the Goldstein-distribution method are 90.3% and 18.5%, respectively, indicating that the results are completely distorted. Moreover, the error in the commonly used heavy-load condition for ducted propellers (low advance coefficient J) is higher than that in the light-load condition. In Table 4, the total thrust coefficient K_{TT} is the sum of K_{TP} and K_{TD}. When the Goldstein-distribution method is applied, the K_{TT} under each advance coefficient is about 30% smaller than the test value, representing a large error. In contrast, the errors in the K_{TT} obtained by the two improved methods are only about 5%. Specifically, the case of J = 0.7 is not considered in the calculation of the average relative error as it is beyond the design advance coefficient range and results in a significant error in K_{TT}.

The flow velocity distributions of the ducted propeller based on the improved BFMs are shown in Fig. 11. Depending on the different forms of body force distribution, the flow velocity under Distribution 1 (uniform distribution) is rather uniformly distributed in the radial direction, while the flow velocity under Distribution 2 increases with the radial distance. The duct thrust coefficient K_{TD} is almost the same while the propeller thrust coefficient K_{TP} differs under the two forms of body force distribution. The reason is that these two forms of distribution have a small influence on the flow field near the duct that is decisive to the duct thrust but have a large influence on the flow field in the region where the propeller (inflow plane) is located. The improved BFM 1 simulates K_{TP} more accurately than the improved BFM 2. However, the small K_{TP} values obtained by the two methods are related to the simple processing in the BFMs of taking the average velocity on a selected inflow plane as the advance velocity. In summary, the improved BFMs numerically simulate the hydrodynamic performance of a ducted propeller in open water effectively and are superior to the traditional BFM. Therefore, they can lay a foundation for accurately simulating the hydrodynamics of the interaction between the hull and the ducted propeller (body force).

5.2 Hydrodynamic performance of interacting vehicle and ducted propeller based on improved BFMs

The proposal of the body force model for ducted propellers is ultimately aimed at improving the accuracy and efficiency of numerical simulation of vehicles equipped with ducted propellers. In this section, the simulation values of the ducted BFM are compared with those of the discretized ducted propeller model equipped with a revolution body to further explore the applicability of the improved BFMs 1 and 2 behind an underwater vehicle. In the

Table 4 Total thrust coefficients of ducted propeller in open water

Advance coefficient J	Total thrust coefficient K_{TT}			Test value	Relative error/%		
	Goldstein-distribution method	Improved BFM 1	Improved BFM 2		Goldstein-distribution method	Improved BFM 1	Improved BFM 2
0	0.353 4	0.499 8	0.506 9	0.521 9	−32.28	−4.24	−2.87
0.1	0.316 3	0.434 6	0.442 8	0.467 3	−32.29	−7.00	−5.24
0.2	0.282 6	0.376 0	0.386 0	0.413 8	−31.70	−9.14	−6.71
0.3	0.247 1	0.331 5	0.341 1	0.360 3	−31.42	−7.99	−5.34
0.4	0.216 3	0.284 6	0.294 7	0.303 9	−28.81	−6.36	−3.04
0.5	0.180 4	0.236 9	0.245 3	0.247 5	−27.09	−4.29	−0.86
0.6	0.132 6	0.185 9	0.192 5	0.185 1	−28.37	0.40	4.01
0.7	0.062 3	0.131 0	0.134 1	0.110 8	−43.80	18.20	20.94
|Average|					30.20	5.60	4.00

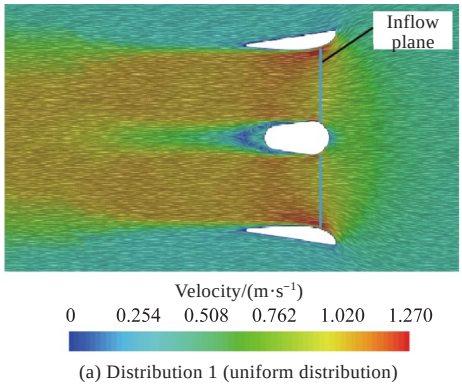

(a) Distribution 1 (uniform distribution)

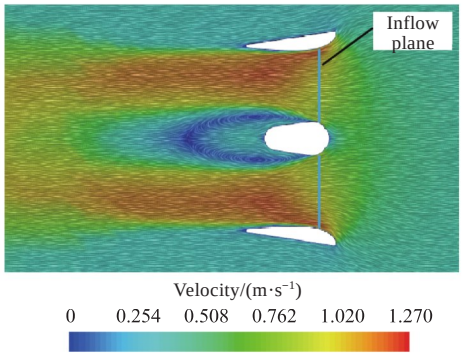

(b) Distribution 2

Fig. 11 Flow velocity distributions of ducted propeller in open water based on improved BFMs (J = 0.3)

simulation, the assembly remains stationary, and the rotational speed of the propeller is kept constant at 1 500 r/min. Hydrodynamic performance under different conditions is calculated by adjusting the inflow velocity. The performance curves of the propeller thrust T_P, duct thrust T_D, resistance f_m on the revolution body, and mass flow rate Q are shown in Fig. 12. In the figure, the discretized ducted propeller is the condition where the discretized ducted propeller model is equipped with a revolution body; the subscript B is the condition behind an underwater vehicle to distinguish it from the open-water condition; subscripts 1, 2, and G are the improved BFM 1, improved BFM 2, and Goldstein-distribution method, respectively.

According to Fig. 12, the Goldstein-distribution method and the improved BFMs 1 and 2 achieve an average relative error of −12%, 1.3%, and 14.0%, respectively, in propeller thrust T_P relative to the values of the discretized ducted propeller behind an underwater vehicle; the duct thrust T_D, mass flow rate Q, and especially the resistance f_m on the revolution body obtained by the improved BFMs 1 and 2 agree well with the corresponding simulation values of the discretized ducted propeller behind an underwater vehicle, and the relative errors are merely around 0.5%, representing a significant increase in accuracy compared with that of the Goldstein-distribution method. The simulation accuracy of the mass flow rate affects not only the duct thrust but also the pressure field at the tail of (resistance on) the revolution body. The accurate prediction of the hydrodynamic performance of the interacting hull and ducted propeller by the improved BFMs can lay the foundation for simulating the maneuverability dynamics of underwater vehicles. Moreover, as shown in Figs. 12(b) to 12(d), the errors in the duct thrust T_D, resistance f_m on the revolution body, and mass flow rate Q obtained by the Goldstein-distribution method relative to the corresponding values of the discretized propeller model gradually decrease as the inflow velocity increases. This phenomenon can be attributed to the fact that the hydrodynamic pitch angle of the propeller decreases as the advance velocity increases, and the hydrodynamic effect of the blade lift simulated by the body force source weakens accordingly, further leading to a weakened hydrodynamic effect of the interacting propeller and duct. As a result, the errors caused by the distorted simulation of the interaction effect

decrease as well.

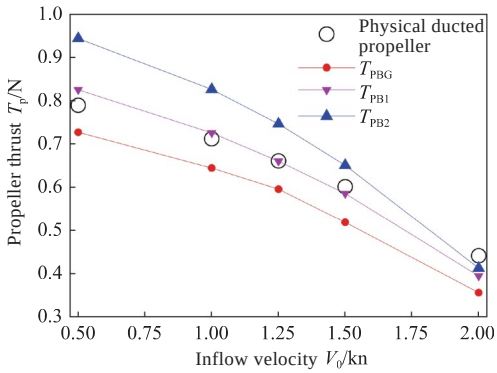

(a) Propeller thrust

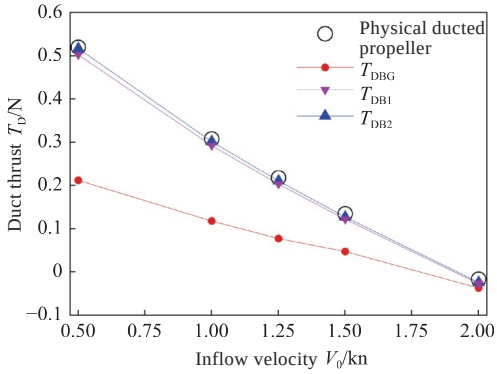

(b) Duct thrust

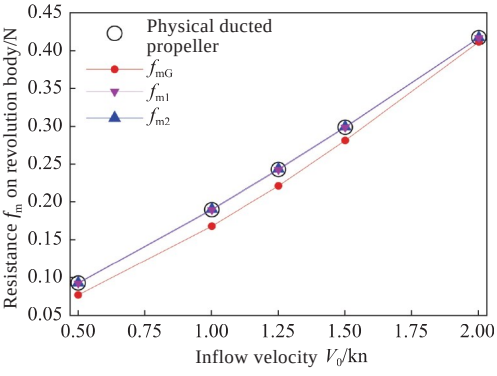

(c) Resistance on revolution body

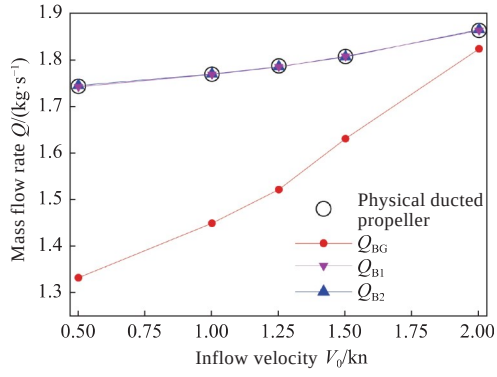

(d) Mass flow rate

Fig. 12 Comparison of performance curves of ducted propeller behind revolution body based on by improved BFMs

As can be seen from Table 5, the absolute average relative errors in the resultant forward force obtained by the improved BFMs 1 and 2 under each inflow velocity (excluding 2 kn) are 1.86% and 11.65%, respectively, which are significantly lower than the absolute average relative error in the value calculated by the Goldstein-distribution method (30.28%). Similar to the case under open-water conditions, the improved BFM 1 still achieves high accuracy behind an underwater vehicle and is thus superior to the improved BFM 2. In summary, the improved BFMs generally numerically simulate the hydrodynamic performance of a ducted propeller behind an underwater vehicle effectively. Their computational accuracy is substantially higher than that of the Goldstein-distribution method and is also superior to that of the traditional BFM. As a result, they are readily applicable to the numerical simulation of the hydrodynamic performance of an interacting hull, duct, and body force model.

As mentioned in the last section, a large error can be observed in the simulated thrusts from the ducted propeller obtained by the BFMs (Table 4) when the advance coefficient is large ($J \geqslant 0.7$) under open-water conditions. According to Fig.12(a), Fig.12(b), and Table 5, this is also the case under a high inflow velocity (2 kn) behind an underwater vehicle. This issue will now be discussed. The propeller lift will decrease under a large advance coefficient (larger than the value when the duct thrust becomes a resistance), and the "dynamic hydrodynamic effect" between the propeller and the duct decreases accordingly. For ease of understanding, the authors assume that the propeller stops rotating, remains stationary inside the duct, and endures the impact of the high-velocity inflow. The BFMs simulate the lifting effect of the propeller by replacing the blades with a body force source. In the case of a high advance velocity, the blades play more of a resistance role, and the effect between the propeller and the duct is more of a "stationary hydrodynamic effect". The currently available BFM fails to simulate the blockage effect of the propeller. For the above reason, Yu et al. [10] conducted a correction study by focusing on the blockage effect of the blades in the BFM. In addition, as the advance velocity increases, vortex shedding and other flow phenomena of the duct need to be captured to accurately evaluate the hydrodynamic characteristics of the duct, and this effort is equivalent to simulating a hydrofoil with a large attack angle. Nevertheless, the RANS method used in this study is not competent enough for the task.

However, ducted propellers are generally designed

for heavy-load conditions (low advance coefficients) characterized by large thrusts and high efficiency. A high advance coefficient results in severe flow separation, low efficiency, and transformation of the thrust from positive to negative (the resistance takes form). Relatively speaking, the simulation of heavy-load conditions is the focus of the research on the hydrodynamic performance of a ducted propeller and also the focus of this study.

Under the condition where the ducted propeller is behind an underwater vehicle, the propeller thrust (or resultant forward force) obtained by the improved BFM 2 deviates more from the simulation values of the discretized model than the propeller thrust (or resultant forward force) obtained by the improved BFM 1. This phenomenon can be attributed to the simplification of the advance velocity on the inflow plane in this study. The velocity distributions of the ducted propeller behind an underwater vehicle obtained by the improved BFMs are shown in Fig. 13. The axial position of the selected inflow plane is marked in the left part of the figure and the distribution of the dimensionless axial velocity on the inflow plane is illustrated in the right part of the figure (the velocity is non-dimensionalized at its maximum value). As shown in the figure, the velocity contours inside the duct obtained by the improved BFM 1 (Fig. 13(a)) are loose and uniformly distributed; in contrast, those obtained by the improved BFM 2 (Fig. 13(b)) are dense and distributed in a non-uniform manner. In this study, the overall average axial velocity on the inflow plane is taken as the advance velocity of the propeller. The influence of the spatial non-uniformity of the inflow on the hydrodynamic performance of the ducted propeller is neglected, resulting in the failure of the body force source to be distributed according to the local advance velocity. In the follow-up research, the local velocity at each radius can be taken as the advance velocity to distribute the body force source, and the distribution of the external inflow velocity needs to be considered. The uniformly distributed body force can serve as compensation for the simplification of the advance velocity on the inflow plane because it alleviates the non-uniform distribution of the inflow and achieves high simulation accuracy.

Table 5 Resultant forward force on vehicle−propeller behind an underwater vehicle

Inflow velocity/kn	Resultant forward force/N			Simulation value of physical model/N	Relative error/%		
	Goldstein-distribution method	Improved method 1	Improved method 2		Goldstein-distribution method	Improved BFM 1	Improved BFM 2
0.50	0.863 8	1.237 1	1.370 4	1.219 0	−29.13	1.48	12.42
1.00	0.595 9	0.830 9	0.939 7	0.831 7	−28.35	−0.10	12.97
1.25	0.453 1	0.622 6	0.714 9	0.637 5	−28.92	−2.33	12.13
1.50	0.286 5	0.410 4	0.478 8	0.439 0	−34.73	−6.50	9.08
2.00	−0.090 5	−0.047 3	−0.029 3	0.008 6	−1 152.30	−650.00	−440.70
|Average|					30.28	1.86	11.65

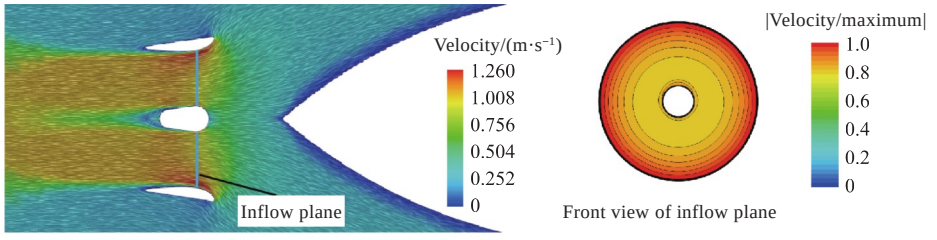

(a) Distribution 1 (uniform distribution)

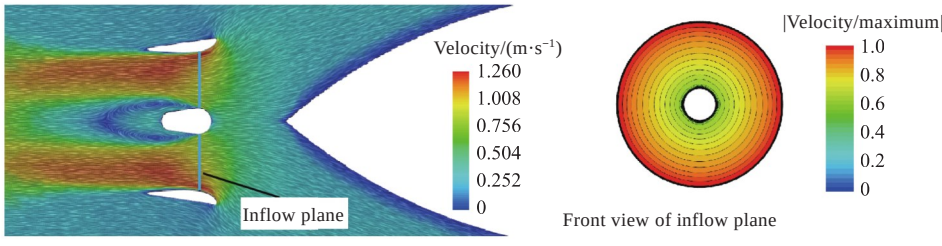

(b) Distribution 2

Fig. 13 Flow velocity distribution of vehicle-ducted propeller based on improved BFMs (inflow velocity: 0.5 kn)

6 Conclusions

In this study, the RANS method was used to study the applicability of the Goldstein-distribution method to the simulation of the hydrodynamic performance of a No.19A+Ka4-70 ducted propellers. The wing theory was employed to determine the reason for the inaccurate simulation result of the hydrodynamic performance of the ducted propeller. Then, correction theory and methods were proposed from the perspectives of the mass flow and the body force distribution model. Finally, the improved BFMs are numerically validated in open water and behind condition. The main conclusions are as follows:

1) The simulation accuracy of the Goldstein-distribution method is relatively low when the internal flow inside the duct is studied. The improved BFMs, based on the principle of equal mass flow, introduce a correction coefficient to correct the mass flow of the ducted propeller (duct with the body force propeller). On this basis, the flow field in the duct in the above model can share the same macroscopic characteristics as those of the flow field in the duct in the discretized ducted propeller. In this way, efficient and accurate improved BFMs applicable to ducted propeller are obtained.

2) Regarding the improved BFMs for ducted propellers proposed in this study, the uniform body force source distribution (improved BFM 1) provides high simulation accuracy both in open water and behind an underwater vehicle.

3) By introducing the mass flow correction, the improved BFMs can effectively simulate the interaction between the propeller (the body force source) and the main body of underwater vehicle. Furthermore, the accuracy of the improved BFM is comparable to the discretized propeller method in terms of hull resistance and ducted propeller thrust. Significance improvement can be observed compared with the Goldstein-distribution method.

4) Although the improved BFMs can obtain a more accurate propeller thrust, they require more information about the ducted propeller itself than the Goldstein-distribution method, such as the relationship between the speed and the mass flow inside the duct. However, this cost is negligible compared with the high time consumption required to simulate the dynamic maneuverability of a vehicle equipped with a discretized ducted propeller.

References

[1] HOUGH G R, ORDWAY D E. The generalized actuator disk [R]. Ithaca, NY: Therm Advanced Research Inc, 1964.

[2] WU Z H, CHEN Z G, DAI Y, et al. Numerical study of hydrodynamic force on ships in turning motion based on a body-force propeller model [J]. Chinese Journal of Ship Research, 2013, 8(4): 12−19 (in Chinese).

[3] HUANG C R. Direct simulation of maneuver of the underwater vehicle based on overset grid [D]. Wuhan: Wuhan University of Technology, 2018 (in Chinese).

[4] GAGGERO S, VILLA D, TANI G, et al. Propeller nozzles design using viscous codes and optimization algorithms [C]//VII International Conference on Computational Methods in Marine Engineering-MARINE 2017, 2017.

[5] HE T, FENG D K, ZHANG H, et al. Numerical simulation of full-scale ship turning motion [J]. Shipbuilding of China, 2020, 61(Supp 2): 52−63 (in Chinese).

[6] WU H, OU Y P, XIANG G. Research on the influencing factors of body force method in numerical simulation of ship self-propulsion [J]. Journal of Wuhan University of Technology (Transportation Science & Engineering), 2017, 41(2): 273−276 (in Chinese).

[7] GOLDSTEIN S. On the vortex theory of screw propellers [J]. Proceedings of the Royal Society A: Mathematical, Physical and Engineering Sciences, 1929, 123 (792): 440−465.

[8] WU J M, LAI Y F, LI J W, et al. Distribution characteristics of thrust, advanced and induced velocity on ducted propeller disk [J]. Ship Engineering, 2016, 38(12): 23−26, 36 (in Chinese).

[9] FENG D K, YU J W, RAN HE R, et al. Improved body force propulsion model for ship propeller simulation [J]. Applied Ocean Research, 2020, 104: 102328.

[10] YU C, DONG X Q, YANG C J. A body force model for tunnel thrusters and application [J]. Journal of Shanghai Jiao Tong University, 2018, 52(3): 291−296 (in Chinese).

[11] ESLAMDOOST A, VIKSTRÖM M. A body-force model for waterjet pump simulation [J]. Applied Ocean Research, 2019, 90: 101832.

[12] KNIGHT B G, MAKI K J. A semi-empirical multi-degree of freedom body force propeller model [J]. Ocean Engineering, 2019, 178: 270−282.

[13] SONG C H, LIN Y F, CHEN W X, et al. CFD analysis for the ducted tail rotor based on momentum-source method [J]. Helicopter Technique, 2009(1): 6−11 (in Chinese).

[14] YANG L, FENG J, SUN W Y, et al. Research on interaction between hybrid CRP pod and hull of large vessel [J]. Shipbuilding of China, 2019, 60(2): 59−68 (in Chinese).

[15] MENTER F R, KUNTZ M, LANGTRY R B. Ten

years of industrial experience with the SST turbulence model [C]//Turbulence, Heat and Mass Transfer. Antalya: Begell House, 2003.

[16] WILCOX D C. Formulation of the *k*-ω turbulence model revised [J]. AIAA Journal, 2008, 46(11): 2823−2838.

[17] SHENG Z B, LIU Y Z. Ship theory [M]. Shanghai: Shanghai Jiao Tong University Press, 2003: 46−47 (in Chinese).

[18] PANG Y J, WANG Y X, YANG Z Y, et al. Direct route drag calculation and shape optimization of Myring shape axisymmetric revolution body [J]. Journal of Harbin Engineering University, 2014, 35(9): 1093−1098 (in Chinese).

基于改进体积力法的导管螺旋桨水动力性能数值研究

王浩天[1],向巩[*1,2,3,4],袁在思[1],向先波[1,3,4]

1 华中科技大学 船舶与海洋工程学院,湖北 武汉 430074

2 浙江大学 流体动力与机电系统国家重点实验室,浙江 杭州 310027

3 华中科技大学 船舶和海洋水动力湖北省重点实验室,湖北 武汉 430074

4 高新船舶与深海开发装备协同创新中心,上海 200240

摘　要:[**目的**]旨在解决传统Goldstein体积力法在导管螺旋桨水动力仿真中的适用局限性问题。[**方法**]首先,基于机翼理论,分析导管水动力模拟失真的原因,并以质量流量和体积力分布模型为切入点,提出修正思想和方法;然后,采用RANS方法探究经质量流量修正后的2种体积力分布模型的模拟精度。[**结果**]结果显示,2种改进体积力法在敞水工况下其总推力系数的平均相对误差均为5%左右;在艇后工况下,前进合力的平均相对误差分别为1.8%和11.6%。[**结论**]研究表明,基于改进体积力法的导管螺旋桨在敞水和艇后工况下的模拟精度较传统体积力法有较大的提升,能准确实现对导管螺旋桨水动力性能的数值模拟,可为水下航行器高效、动态的操纵性仿真奠定基础。

关键词:改进体积力法;导管螺旋桨;流量修正;分布修正;计算流体动力学